Experimental Determination of Temperature Profiles by Ground-Based Microwave Radiometry

E. R. WESTWATER AND J. B. SNIDER

Wave Propagation Laboratory, ERL, NOAA, Boulder, Colo. 80302

A. V. CARLSON

Atmospheric Sciences Laboratory, U. S. Army Electronics Command, White Sands Missile Range, N. Mex. 88002

(Manuscript received 12 April 1974, in revised form 3 February 1975)

ABSTRACT

A one-week experiment was conducted to evaluate a dual-frequency microwave radiometer for recovering low altitude temperature profiles; the two-channel radiometer operated at 53.5 and 54.5 GHz. Meteorological support included radiosondes, helicopters, and an instrumented 150 m tower. Statistical inversion of 13 radiometer angular scan data sets resulted in an average rms error of 2.0 K up to 3 km for the microwave system. Significant features of thermal inversion structure were recovered. A continuous set of fixed-angle brightness observations correlated well with temperatures measured on the tower.

The statistical inversion method and the Backus-Gilbert method were applied to the analysis of the accuracy and the spatial resolution of the ground-based system. Model calculations were performed to estimate the effects of departures from horizontal stratification and of significant time variation in temperature structure during an elevation scan.

1. Introduction

Ground-based passive sensing of temperature profiles is an increasingly active field of research (Westwater, 1972a; Snider, 1972; Mount *et al.*, 1969; Waters, 1971; Miner *et al.*, 1972). In this paper we present the results of a one-week experiment designed to evaluate a dual-frequency microwave radiometric technique to retrieve thermal profiles. Participants in this experiment, held at White Sands Missile Range during the period 15–19 May 1972, were the Wave Propagation Laboratory of NOAA and the Atmospheric Sciences Laboratory of the U. S. Army Electronics Command.

Brightness temperatures were measured by a two-channel microwave radiometer operating at 53.5 and 54.5 GHz in a variable elevation angle mode. Retrieved profiles were compared with direct soundings of temperature structure made by radiosondes, helicopter flights, and temperature sensors located on a 150 m meteorological tower. Particular emphasis in the experiment was placed on the ability of the radiometric technique to recover significant features of low-altitude profiles, such as the height and intensity of ground-based inversions. In addition, it was considered important to differentiate between unstable and stable conditions by radiometric means. Consequently, the times at which soundings were made were chosen to insure that we observed the transition from nocturnal inversion to lapse conditions and vice versa.

To facilitate the data analysis and interpretation, various numerical studies are presented. To aid in interpreting profile retrievals, we studied vertical resolution via the Backus-Gilbert formalism, and expected error in retrieving via the statistical inversion method. Since tower temperature measurements occasionally indicated significant changes in the profile during an elevation scan, we computed these effects on the brightness angular spectrum for a few models.

2. Radiative transfer

Passive remote sensing of atmospheric profiles by radiometric techniques requires a functional relationship between measurements of radiant power and desired profile parameters. This relationship usually requires the solution of two problems in radiative transfer: (i) the direct problem; i.e., given the state of the atmosphere (temperature and composition profiles, etc), what is the radiant power?, and (ii) the indirect problem; i.e., given a set of radiation measurements, what is the state of the atmosphere? The solution of (ii) almost always requires the solution of (i). In this section we briefly review the formal solution to the direct problem, namely the radiative transfer equation, and discuss the uncertainties in calculations based on this equation.

The downward spectral brightness temperature T_b, emitted by a non-scattering atmosphere in local thermo-

dynamic equilibrium is given by

$$T_{b\nu}=(T_{b\nu}^{\text{ext}})\tau_\nu-\int_0^\infty T\frac{d\tau_\nu}{ds}ds, \tag{1}$$

where:

$T_{b\nu}^{\text{ext}}$ brightness temperature external to the atmosphere (K)
τ_ν transmission function
ν frequency (GHz)
T absolute temperature (K)
s path length from surface to emitting volume (km).

In general, the transmission τ_ν is a strong function of atmospheric composition and depends only weakly on temperature. Microwave absorption in the clear atmosphere is due principally to rotational transitions of O_2 (0.5 cm) and H_2O (1.35 cm).

Although (1) represents the exact solution to the transfer equation, the functional dependence of τ_ν on atmospheric parameters must be specified before one can calculate $T_{b\nu}$, from radiosonde observations, for example. The absorption characteristics of a gas depend on such molecular characteristics as line strengths and positions, spectral line shape, foreign and self-collision broadening parameters, etc. The details of our calculations are given by Westwater *et al.* (1973). We use the Van Vleck-Weisskopf line shape with parameters for O_2 given by Carter *et al.* (1968), and parameters for H_2O given by Westwater (1967). The accuracy of the O_2 calculations is about 8%.

Because of the importance of an all-weather capability in a remote sensing system, the effect of clouds and rain should be discussed. As shown in Section 9, clouds showed small effect on the microwave measurements during the periods of measurement. In general, however, microwaves are affected by clouds in a manner that depends on the liquid water content and drop size distribution of the cloud (Westwater, 1972b). For nonprecipitating clouds, excellent possibilities exist to correct their effect on the total brightness temperature to give an equivalent clear air measurement. This might be achieved, for example, with a radiometer operating at say, 31 GHz, where the atmospheric emission is weakly affected by temperature and water vapor but is sensitive to clouds. A similar technique has been successful in separating water vapor and cloud emission observed from a satellite (Staelin *et al.*, 1973). The effect of rain, however, is large and would be difficult, if not impossible, to correct.

3. Inversion techniques and expected accuracy

The operational feasibility of radiometers as remote sensors of temperature profiles depends on the analytical technique used to extract profiles from radiance observations. As in many complex problems, there is no one "best" method for all situations. For example, iterative techniques that require large computer facilities would be impractical for a small field instrument whose purpose is to provide real-time profiles. On the other hand, a statistical technique allows great simplification for a real-time operation but requires a history of profiles that may not be available. In this section we discuss and compare inversion techniques that are later used in the analysis of radiometer data. A discussion of many mathematical aspects of the inversion problem is given by Westwater and Strand (1972). In addition, Colin (1972) has edited a compilation of profile inversion techniques in many fields of physics.

Statistical inversion techniques use radiation measurements to estimate, in some sense, most probable profile parameters. Although other estimation procedures are possible, we confine our attention to minimum variance estimation. Let $\mathbf{d}$ be an n-component vector of measurements (data) and $\mathbf{p}$ an m-component vector of profile parameters. For example, $\mathbf{d}$ could be a set of brightness temperatures and surface meteorological observations, while $\mathbf{p}$ could represent a temperature profile at m specified altitudes. Let the ensemble averages of a quantity V be $\langle V\rangle$ and the departure of V from its average be $V'=V-\langle V\rangle$. Furthermore, we denote the estimate of $\mathbf{V}'$ by $\hat{\mathbf{V}}'$. Then the minimum variance unbiased estimator of $\mathbf{p}$ as a linear function of $\mathbf{d}$ is (Deutsch, 1965)

$$\hat{\mathbf{p}}'=\langle\mathbf{p}'\mathbf{d}'^*\rangle\langle\mathbf{d}'\mathbf{d}'^*\rangle^{-1}\mathbf{d}'. \tag{2}$$

Here, the asterisk represents matrix transposition.

Our first inversion technique used (2) directly (see Section 9). We obtained an ensemble of 261 radiosonde profiles representing five years of May soundings at White Sands Missile Range. In contrast to many National Weather Service soundings, which are taken at 0000 and 1200 GMT, these soundings were more or less evenly distributed throughout 24 h. The brightness temperatures $\mathbf{T}_b$ at 53.5 and 54.5 GHz and 15 selected elevation angles were calculated as discussed in Section 2 for each profile in the ensemble. These 30 values plus surface observations of temperature T_0, pressure P_0 and humidity r_0 were combined to form a 33-component data vector $\mathbf{d}=[\mathbf{T}_b^*|T_0,P_0,r_0]^*$. The average of $\mathbf{d}$ was simply obtained by averaging each component over the ensemble

$$\langle\mathbf{d}\rangle\approx\frac{1}{N}\sum_{i=1}^{N}(\mathbf{d})_i, \tag{3}$$

where i refers to a member of the ensemble and N is the total number of profiles. The cross covariance matrix, $\langle\mathbf{T}'\mathbf{d}'^*\rangle$, between the temperature at m fixed altitudes and $\mathbf{d}$ was calculated by

$$\langle\mathbf{T}'\mathbf{d}'^*\rangle\approx\frac{1}{N-1}\sum_i(\mathbf{T}-\langle\mathbf{T}\rangle)_i(\mathbf{d}-\langle\mathbf{d}\rangle)_i^*. \tag{4}$$

In (4), we assumed experimental errors in $\mathbf{d}$ were

uncorrelated with $\mathbf{T}$. To calculate $\langle \mathbf{d}'\mathbf{d}'^* \rangle$ from past soundings in a way that could be applied directly to our experimental situation required knowledge of the noise properties of the radiometer. We assumed

$$\mathbf{d} = \mathbf{d}^{(\mathrm{atm})} + \boldsymbol{\varepsilon}, \tag{5}$$

where $\mathbf{d}^{(\mathrm{atm})}$ is the atmospheric contribution and $\boldsymbol{\varepsilon}$ the measurement error, and further, assumed that $\mathbf{d}^{(\mathrm{atm})}$ and $\boldsymbol{\varepsilon}$ were uncorrelated to get

$$\langle \mathbf{d}'\mathbf{d}'^* \rangle = \langle \mathbf{d}'^{(\mathrm{atm})}\mathbf{d}'^{(\mathrm{atm})*} \rangle + \langle \boldsymbol{\varepsilon}\boldsymbol{\varepsilon}^* \rangle. \tag{6}$$

We calculated $\langle \mathbf{d}'^{(\mathrm{atm})}\mathbf{d}'^{(\mathrm{atm})*} \rangle$ from our ensemble using an equation similar to (4). When we inverted radiometer data (see Section 9) the error matrix $\langle \boldsymbol{\varepsilon}\boldsymbol{\varepsilon}^* \rangle$ was estimated from assumed accuracy characteristics of the radiometer and surface observations.

The statistical inversion method allows an *a priori* estimate of the accuracy in remotely inferring profiles. As shown by Westwater and Strand (1968), this accuracy is a function of the number and kind of measurements, the instrument noise levels, and the statistical behavior of profile fluctuations. If we use minimum variance estimation, the residual, $\hat{\mathbf{T}} - \mathbf{T}$, has a covariance matrix given by (Morrison, 1967)

$$\langle (\hat{\mathbf{T}} - \mathbf{T})(\hat{\mathbf{T}} - \mathbf{T})^* \rangle = \langle \mathbf{T}'\mathbf{T}'^* \rangle - \langle \mathbf{T}'\mathbf{d}'^* \rangle \langle \mathbf{d}'\mathbf{d}'^* \rangle^{-1} \langle \mathbf{d}'\mathbf{T}'^* \rangle. \tag{7}$$

The square root of the ith diagonal element of this matrix represents the standard deviation of the inferred profile at the ith altitude. Figs. 1 and 2 show calculations of (7) for the data vector $\mathbf{d}$ of various combinations of brightness observations plus errorless surface measurements T_s, P_s, r_s. The noise matrix $\langle \boldsymbol{\varepsilon}\boldsymbol{\varepsilon}^* \rangle$ was assumed to be diagonal with brightness variance $= (1.0\ \mathrm{K})^2$. Fig. 1 compares the residual standard deviation using a total of 30 measurements at 53.5 and 54.5 GHz and 15 measurements at 53.5 GHz, with the *a priori* standard deviation about the mean temperature profile. The residual standard deviation is less than 1.4 K up to 3 km for the multi-channel radiometer. Fig. 2 shows theoretical results using the two single channels vs their combination. Note the 54.5 GHz channel gives consistently more accurate results at all altitudes than 53.5 GHz, while the combination gives moderately better results at all altitudes.

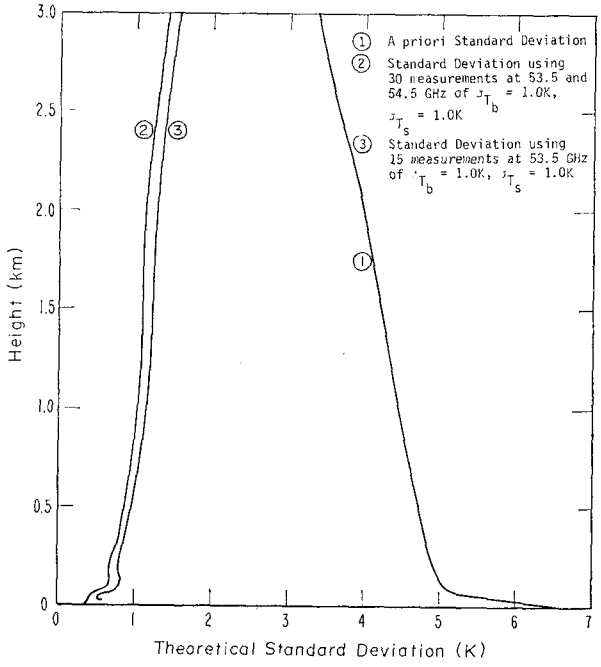

FIG. 1. Theoretical inversion accuracy for various combinations of input data.

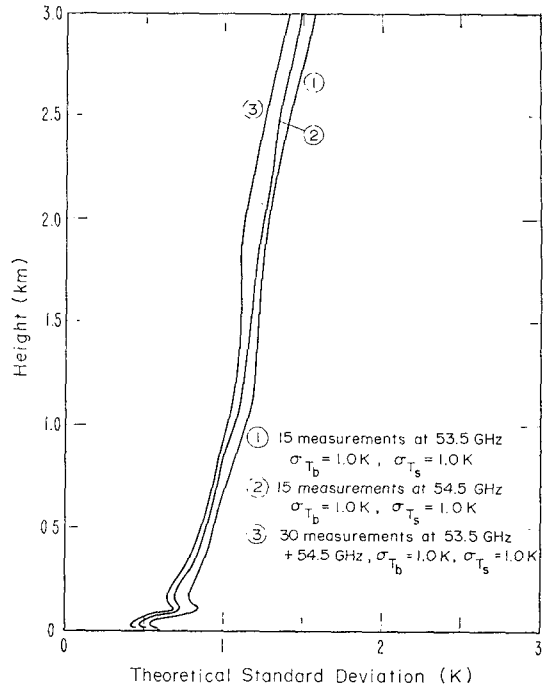

FIG. 2. Theoretical inversion accuracy for two microwave channels and their combination.

As discussed in Section 6, surface measurements were taken about 300 m from the radiometer location. We assume these locations could differ in temperature about 1.0 K and, for the remainder of this paper, we use this value to represent the noise level of the surface temperature observations. In many situations, however, accurate measurements of T_s at the radiometer location would be available. Fig. 3 shows theoretical standard deviations using errorless surface observations vs those of 1.0 K error. As is evident, the retrievals are affected only in the first 60 m above the surface.

The inversion equations (2)–(6) require initially a large amount of computer time. To reduce this time, Westwater (1972a) related a linear approximation of the brightness temperature [Eq. (1)] to the desired

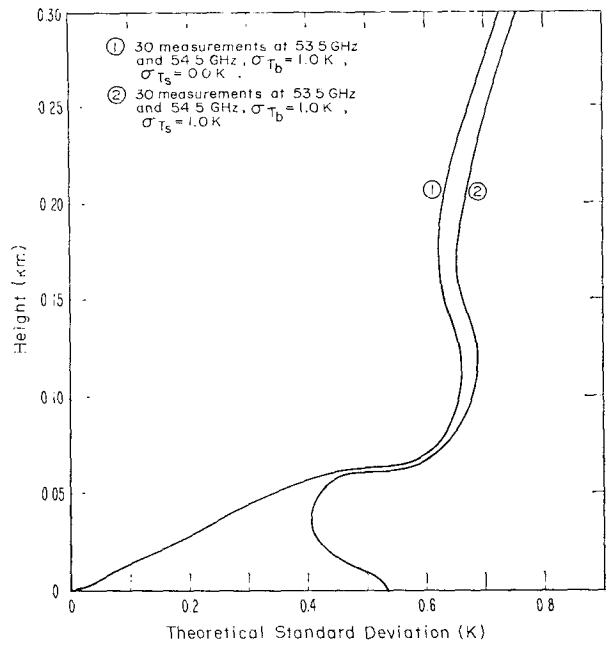

FIG. 3. Theoretical inversion accuracy with and without error in the surface temperature measurement.

profile fluctuations. This procedure requires calculations of brightness temperature and its derivative with respect to temperature, pressure and humidity for the average profile only. If we define the $n\times m$ matrix

$$(A_T)_{ij}=\left.\frac{\partial T_{bi}}{\partial T_j}\right|_{\text{mean profile}} \tag{8}$$

with similar definitions for P and r, then the quantities required by (2) are given by

$$\langle \mathbf{T}'\mathbf{T}_b'^{*}\rangle \approx \langle \mathbf{T}'\mathbf{T}'^{*}\rangle A_{\mathbf{T}}^{*}+\langle \mathbf{T}'\mathbf{P}'^{*}\rangle A_{\mathbf{P}}^{*}+\langle \mathbf{T}'\mathbf{r}'^{*}\rangle A_r^{*}, \tag{9}$$

$$\langle \mathbf{T}_b'\mathbf{T}_b'^{*}\rangle \approx A_T\langle \mathbf{T}'\mathbf{T}'^{*}\rangle A_{\mathbf{T}}^{*}+A_T\langle \mathbf{T}'\mathbf{P}'^{*}\rangle A_{\mathbf{P}}^{*}+\cdots +A_P\langle \mathbf{P}'\mathbf{P}'^{*}\rangle A_{\mathbf{P}}^{*}+\langle \boldsymbol{\varepsilon}\boldsymbol{\varepsilon}^{*}\rangle, \tag{10}$$

$$\langle \mathbf{T}_b\rangle \approx A_T\langle \mathbf{T}\rangle+A_P\langle \mathbf{P}\rangle+A_r\langle \mathbf{r}\rangle. \tag{11}$$

In addition to the direct use of (2), we also used these approximate equations as an inversion algorithm after first calculating means and covariances of meteorological parameters with (2) and (4).

To compare initial computer time requirements for the exact and the approximate inversion algorithms, it can be shown that the total reduction in time achieved by the approximation is approximately $N/(6m)$, where N is the number of profiles. Thus, for five years of twice-a-day soundings, and for 25 height levels, the computer time would be reduced by a factor of about 25.

4. Spatial resolution

The statistical techniques are convenient in predicting the mean square error in an inferred profile as a function of instrument noise levels. Another important quantity is spatial resolution. Recent progress has been made in analysis of indirect sensing systems by the introduction of a quantitative measure of resolution (Backus and Gilbert, 1970). We will summarize below the portions of this theory that we apply to the ground-based temperature problem. A more complete discussion of the technique, as well as other applications, are given by Conrath (1972) and Westwater and Cohen (1973).

The value of a retrieved profile at a given point is representative of some kind of spatial average of the original profile. The effective width, or spread, of the interval over which this average extends is a convenient measure of resolution. If the value of the inferred profile at height h_0 is expressed as the integral of the product of the true function and an averaging kernel, $A(h,h_0)$, then the spread $s(h_0)$, as defined by Backus and Gilbert, is given by

$$s(h_0)=12\int (h-h_0)^2A^2(h,h_0)dh, \tag{12}$$

where the integral extends from the surface to the top of the atmosphere. This measure of resolution is normalized with the factor of 12 so that the spread of a rectangular averaging kernel with width l, height l^{-1}, and centered at h_0, is equal to l. Averaging kernels with suitable localization properties are constructed from the set of known weighting functions appropriate to the inverse problem.

To calculate the spread at various altitudes, we first must determine weighting functions. Ground-based microwave weighting functions $K_i(h)$ for retrieving temperature profiles are (approximately) given by

$$K_i(h)=[\alpha_{\nu_i}(h)/\sin\theta_i]\times\exp\left[-\int_0^h \alpha_{\nu_i}(h')dh'/\sin\theta_i\right], \tag{13}$$

where the subscript i refers to a frequency-angle pair, α_{ν_i} is the absorption coefficient at frequency ν_i, and θ_i is the elevation angle. Fig. 4 shows selected weighting functions (in pressure units rather than height) appropriate to our choice of elevation angles and frequencies.

As Fig. 4 illustrates, the ground-based weighting functions achieve their maximum at the surface. It is not obvious whether linear combinations of these functions will achieve their maxima at higher altitudes and allow a certain degree of spatial resolution. To study this question, we determined from the basis set of 30 weighting functions the (minimum spread) averaging kernels and their associated spreads. The results of these calculations are shown in Fig. 5. Note the extremely narrow resolution near the surface and the broadening of these curves at higher altitudes. Even at 3 km, there is a degree of spatial resolution, although

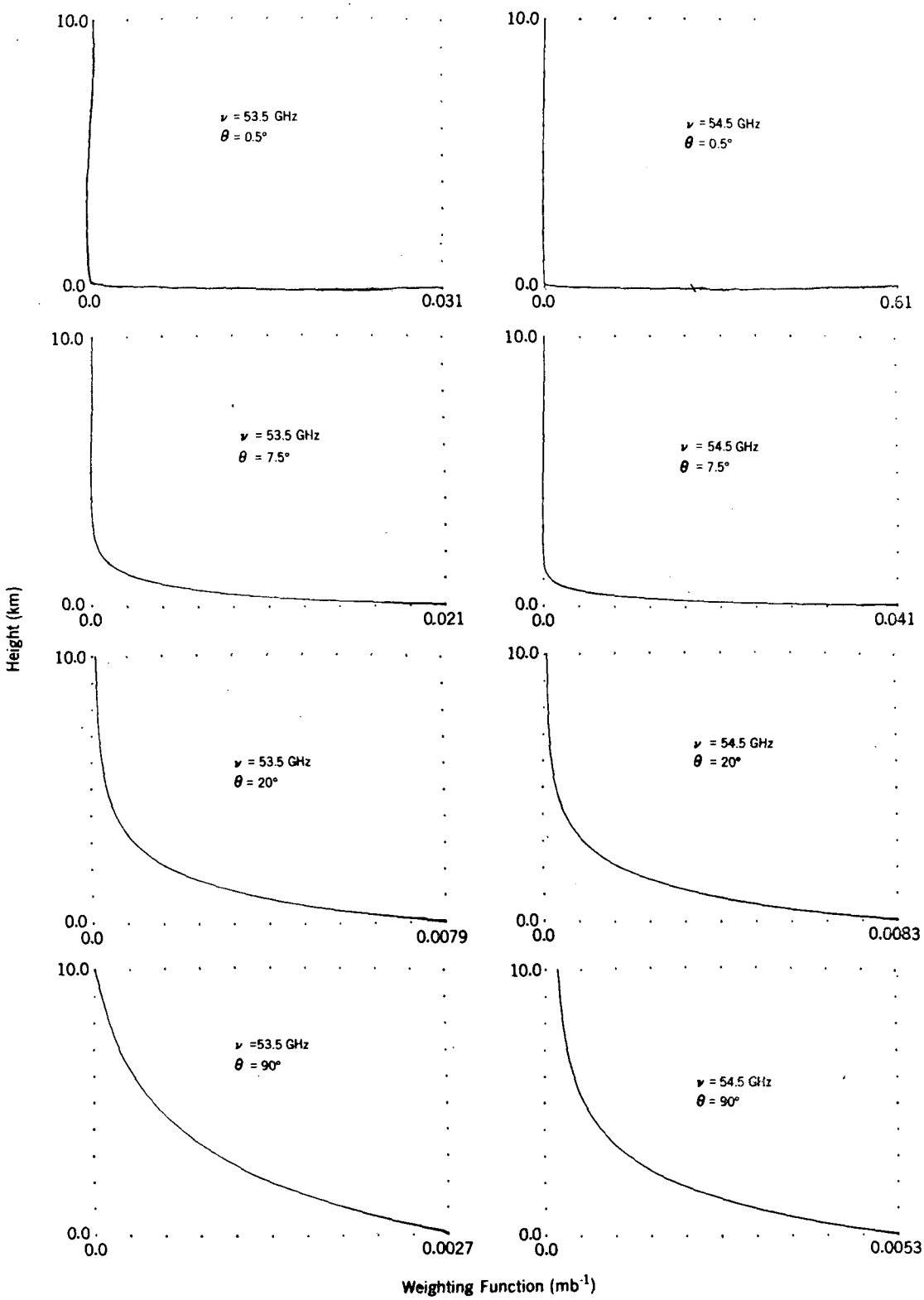

FIG. 4. Ground-based weighting functions at 53.5 and 54.5 GHz.

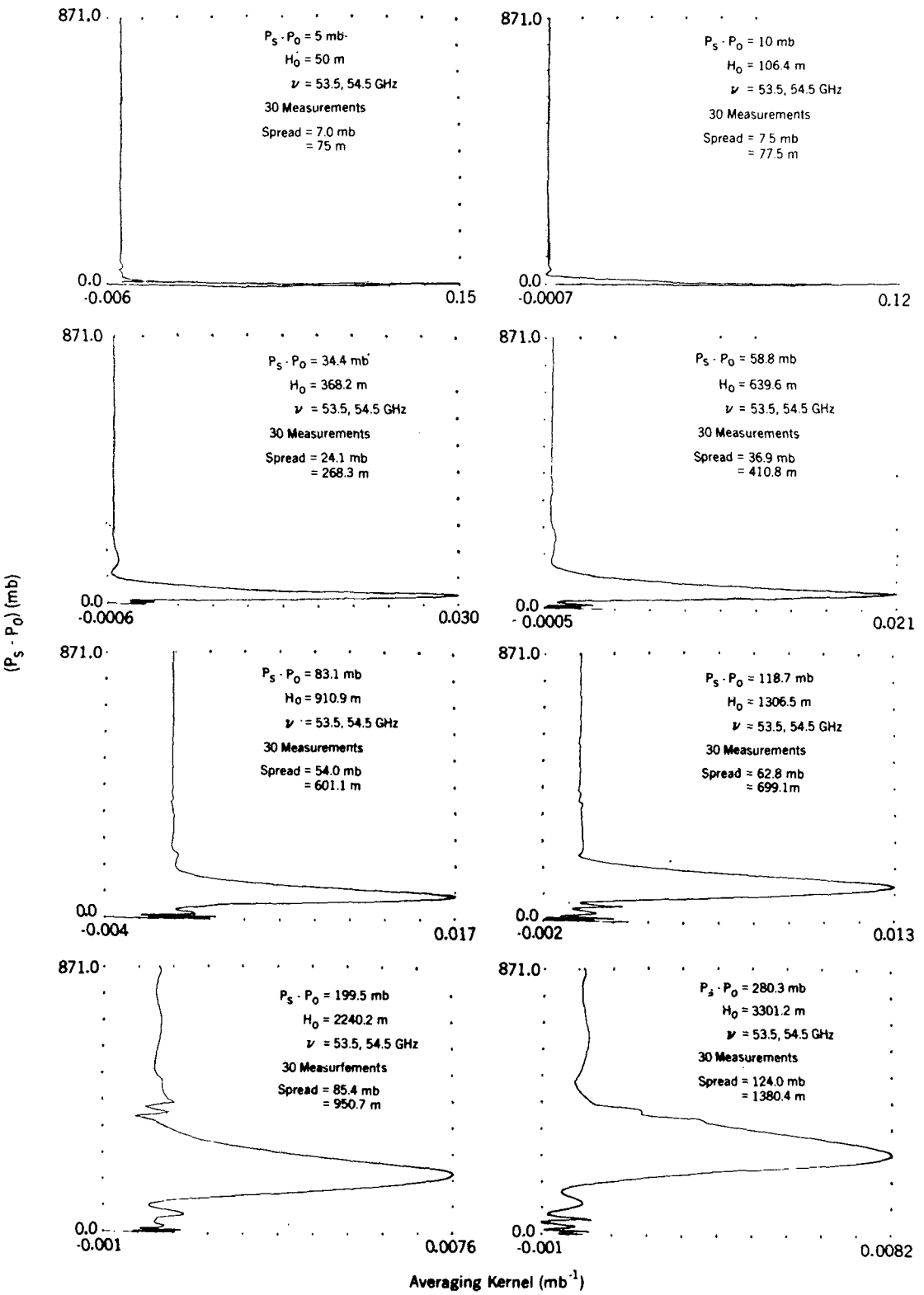

Fig. 5. Averaging kernels for 30 measurements at 53.5 and 54.5 GHz.

fine-structure of retrieved temperature profiles would be smoothed out.

5. Effect of departures from stratification and time stationarity

The angular scan technique of inferring vertical profiles requires horizontal stratification over the spatial region that contributes substantially to the brightness. In addition, since an angular scan requires a finite time to complete, substantial variations in the profile with time can affect the results. In this section, we present model calculations intended to estimate the order of magnitude of these effects.

The local terrain at the field site is uniform in all directions except for the Organ Mountains which lie about 15 km to the west. These mountains frequently induce wave phenomena which propagate downwind through the missile range. To simulate the effect of such a wave on the angular brightness temperature, we assumed a modified profile, $T(x,h)=T_0(h)+A\sin(2\pi x/L)$, where $T_0(h)$ is a standard profile, A the (constant) amplitude, L the wavelength, and x the horizontal coordinate. In Table 1 we show calculations of brightness temperature at 53.5 and 54.5 GHz for $T_0(h)$ as a lapse profile, with wave parameters $A=5.0$ K and $L=2.0$ and 20.0 km. Since the brightness temperature is approximately linear with temperature, numerical values for other choices of A can be estimated by scaling. For low elevation angles, we can compare the numerical results with those obtained from the analytical expression for δT_b when α is constant; namely

$$\delta T_b=A\,(k/\alpha)[1+(k/\alpha)^2]^{-1},$$

where $k=2\pi/L$. For $L=2.0$ and 20.0 km the values obtained from the analytical expression are 0.46 and 2.49 K at 53.5 GHz and 0.88 and 2.11 K at 54.5 GHz.

TABLE 1. Effect of horizontal temperature wave on brightness temperature [K] for $A=5.0$ K.

$$\delta T_b=T_b\left[T_0(h)+A\sin\frac{2\pi x}{L}\right]-T_b[T_0(h)]$$

Elevation angle (deg)	δT_b(53.5 GHz), L 2.0 km	δT_b(53.5 GHz), L 20.0 km	δT_b(54.5 GHz), L 2.0 km	δT_b(54.5 GHz), L 20.0 km
0.5	0.32	2.22	0.72	1.75
2.5	0.39	2.14	0.81	1.69
5.0	0.39	2.11	0.82	1.69
7.5	0.38	2.08	0.82	1.69
10.0	0.36	2.02	0.82	1.68
12.5	0.35	1.97	0.82	1.67
15.0	0.35	1.91	0.83	1.65
20.0	0.33	1.77	0.87	1.65
30.0	0.32	1.58	0.89	1.51
40.0	0.40	1.57	0.97	1.36
50.0	0.58	1.72	1.12	1.22
60.0	0.86	1.89	1.34	1.08
70.0	1.27	1.78	1.66	0.83
80.0	1.74	0.99	1.85	0.39
90.0	0.00	0.00	0.00	0.00
rms error	0.68	1.80	1.40	1.47

TABLE 2. Root mean square errors [K] to 3 km in statistical retrieval of profiles from brightness temperatures calculated from inhomogeneous atmospheres.

Radiometer noise level	Homogeneous atmosphere (lapse profile)	Temperature wave $A=5.0$ K $L=2.0$ km	Temperature wave $A=5.0$ K $L=20.0$ km	Homogeneous atmosphere (elevated inversion)	Cold front model (radiometer 1 km into front)
0.1	0.38	0.95	1.30	1.63	1.66
1.0	0.58	0.47	1.06	1.76	1.78

Another source of temperature inhomogeneity is frontal passage. We investigated a cold air mass moving under warm air with a large frontal slope of 1/50 and a temperature discontinuity across the front of 10 K. The brightness temperature difference between this model and the associated horizontally homogeneous profile depends on the position of the radiometer with respect to the front. With the radiometer 1 and 10 km into the cold sector, the maximum brightness difference exceeds 1 K at only one elevation angle; at 50 km this value had diminished to 0.4 K. These calculations suggest that the effect of departures from horizontal homogeneity induced by even an extreme frontal passage is small, except, perhaps, at the boundary of the front.

To estimate the effect of these departures from stratification on temperature profile recovery, we attempted to retrieve the vertical profiles above the radiometer from brightness temperatures calculated for the inhomogeneous models. For comparison each profile was also retrieved from the brightness temperature calculated from the associated homogeneous model. The results of inverting these data by the statistical technique assuming radiometer noise levels of 0.1 K and 1.0 K, are given in Table 2. As expected, the results for the lower noise level (0.1 K) are more sensitive to stratification errors. Since the statistical inversion equations are linear, the effect of inverting brightness data calculated from similar profiles with different magnitudes of inhomogeneity can be estimated by scaling.

As shown in Section 9, tower measurements occasionally indicated substantial (~4 K) variations of temperature structure during the time of an elevation scan (45 min). Two types of temperature variation occurred: oscillation about a mean value and a linear increase with time. To simulate the effect of such variations on the angular brightness spectrum, we computed the brightness for two cases: in the first, the temperature increased linearly with time a total of 7.5 K during a complete scan; in the second, we allowed $1\frac{1}{2}$ cycles of a sinusoidal variation of amplitude 4 K during the scan. These calculations, plus the brightness spectrum at time zero, are shown in Fig. 6. Note, in one case, the oscillatory behavior of the brightness curve about the spectrum present at time zero. This feature is present in several of the measurements discussed in Section 9.

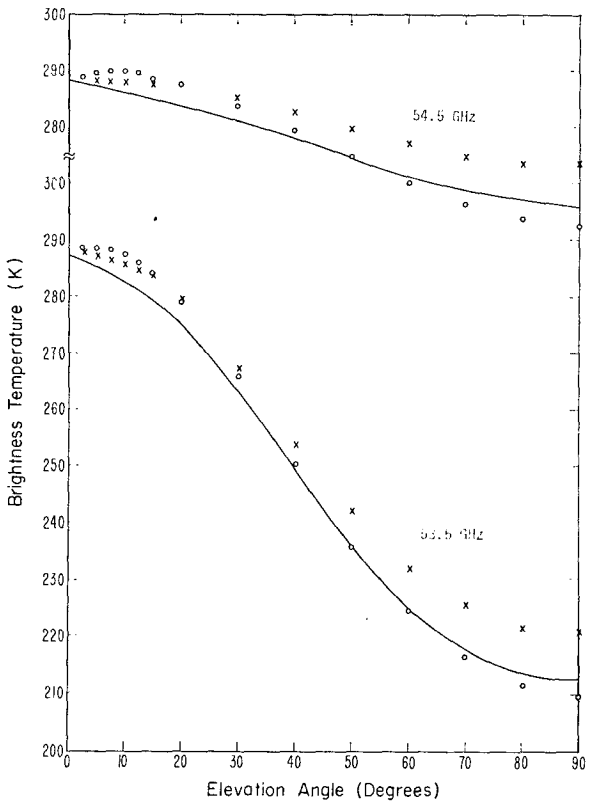

FIG. 6. Effect of time variation in temperature profile on angular brightness spectrum at 53.5 and 54.5 GHz: X's represent a linear increase in temperature with time (a total of 7.5 K during the scan); O's 1½ cycles of a sinusoidal variation of amplitude 4 K during the scan.

6. Experimental plan

Our general objective was to make ground-based remote measurements of the vertical atmospheric temperature profile using a two-channel microwave radiometer as a sensor. Profiles inferred from the radiometric data were to be compared with ground-truth information obtained by radiosondes, tower-mounted temperature sensors, and an instrumented helicopter. Our measurement site was Launch Complex No. 36 on White Sands Missile Range. The radiometer was located 500 m to the west and pointed slightly south of a 150 m instrumented tower. Radiosondes were released 300 m south of the line between the radiometer and tower while the helicopter measurements were made in an area generally south of the tower.

The radiometer measured antenna temperatures at 15 elevation angles ranging from 0° to 90°; since the dwell time at each angle was about 3 min, a complete upward scan required 45 min. A run always began at 0° elevation angle so that the radiometer would probe the lower layers of the atmosphere simultaneously with the launch of the radiosonde.

During radiometer measurements, temperatures were recorded on the tower while the helicopter measured temperature from the surface to approximately 1.5 km, and temperature at constant heights over a horizontal distance of about 8 km. The latter measurements were performed to detect departures from horizontal stratification; measurement heights were 30, 60, 150, 300, 450, 600, 900, 1200 and 1500 m. Helicopter height and position were plotted by a T-9 wind system radar.

Finally, standard surface weather observations of temperature, relative humidity, pressure and cloud cover were recorded at 30 min intervals; these data were recorded approximately 500 m southeast of the radiometer.

A primary task of our investigation was to study the ability of the radiometer to detect the presence and dissipation of temperature inversions. This requirement dictated to a large extent the measurement times; the times selected were 0500, 0800 and 1900 (all times MDT). The 0500 observation was the optimum time to detect inversions because of the strong radiation inversion characteristic of an arid region. The measurement at 0800 was selected because the radiation inversion would probably be in the process of breaking up due to solar heating of the surface and lower atmosphere. Finally, we decided to perform measurements at 1900 (approximately sundown) when the temperature profile could be expected to be in transition from the superadiabatic lapse rate typical of desert afternoons to a more nearly standard lapse condition.

7. Microwave radiometer

The microwave radiometer used to estimate temperature profiles is a two-frequency device designed and constructed in the Wave Propagation Laboratory. The system employs a switchable ferrite circulator which permits operation at two frequencies simultaneously; the system, in effect, consists of two individual switching radiometers (Dicke, 1946) connected to a common antenna and calibration system through a single switch. The radiometer is shown schematically in Fig. 7; a detailed description of the design and performance of the system is given by Snider (1974).

The antenna used with the radiometer is a conical horn reflector with 1.2 m aperture installed in an elevation over azimuth mount (Fig. 8). Antenna axes are individually controlled and the elevation and azimuth angles are displayed and recorded at the radiometer operating position. Antenna half-power beamwidth is approximately 0.3° at our operating frequencies. Primary polarization power patterns were measured to facilitate calculation of brightness temperature.

We derive brightness temperature from antenna temperature using a simple conversion factor based upon our measured antenna characteristics and a mean brightness profile calculated for the geographic area in which measurements are to be made. The process converts antenna temperature measured at a given elevation angle to a line value of brightness temperature at

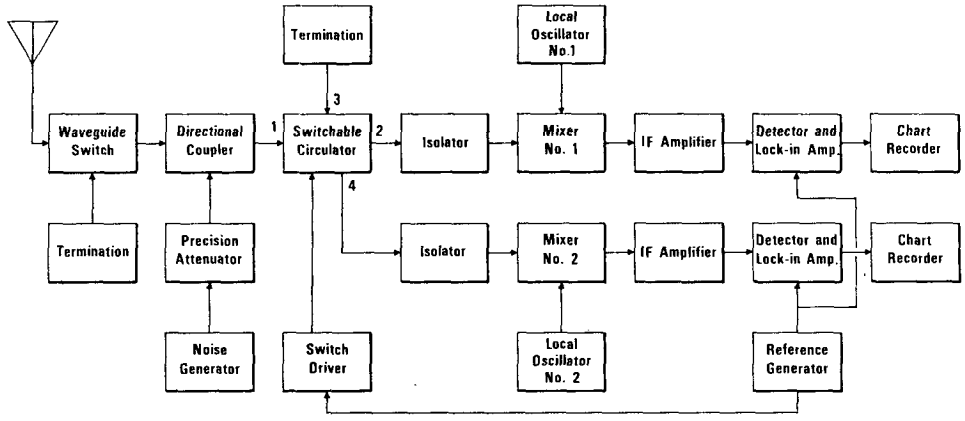

Fig. 7. Block diagram of two-frequency microwave radiometer.

the same elevation angle. We determine the conversion factor by numerically evaluating

$$T_a(\theta)=\frac{1}{4\pi}\int_{4\pi} G(\Omega)T_b(\Omega)d\Omega, \qquad (14)$$

where $T_a(\theta)$ is the integrated antenna temperature at elevation angle θ and $T_b(\Omega)$ and $G(\Omega)$ are the brightness temperature and antenna gain in the direction of solid angle Ω. The mean brightness temperature profiles at our operating frequencies were computed from the history of White Sands radiosonde data described in Section 3. The conversion factor is the difference between mean brightness and the antenna temperature computed using (14). The brightness temperature measurements used as input to the profile retrieval algorithms are calculated from

$$T_{bm}(\theta)=T_{am}(\theta)+[T_b(\theta)-T_a(\theta)], \qquad (15)$$

where $T_{bm}(\theta)$ and $T_{am}(\theta)$ are the measured brightness and antenna temperatures at elevation angle θ, and the quantity in brackets is the conversion factor.

We computed conversion factors using actual brightness profiles measured during the present experiment to estimate the possible error caused by using a mean brightness profile in (14). We found a maximum error of about 1 K for an intense surface-based inversion with the larger differences occurring at the lower elevation angles. The error when measuring a lapse profile was 0.5 K or less at all elevation angles. These calculations indicate that inferred profiles containing temperature inversions may be subject to slightly larger errors than lapse profiles. At the same time, the error is not of sufficient magnitude to justify use of more complex methods (e.g., integral equation inversion) to derive brightness temperature from antenna temperature.

Characteristics of the two-frequency radiometer are summarized in Table 3.

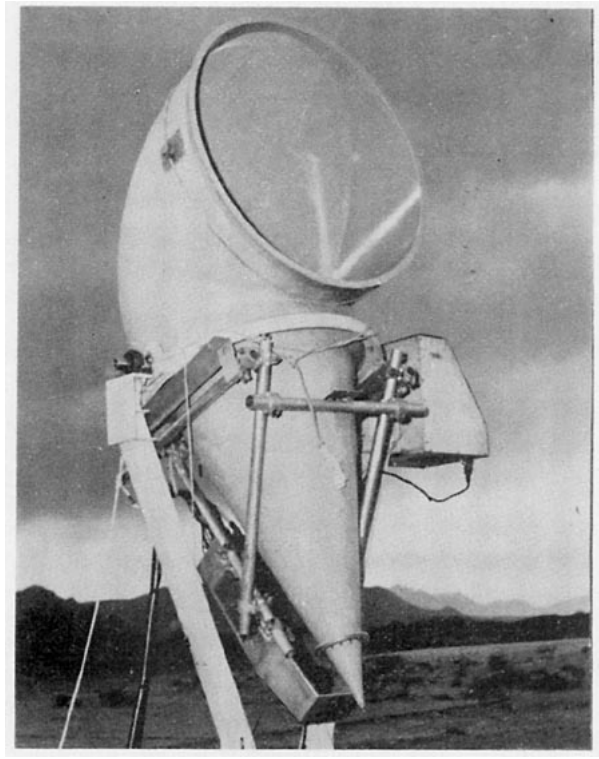

Fig. 8. The two-frequency microwave radiometer and its associated antenna.

8. Meteorological instrumentation

Dry bulb temperatures were measured at eight levels on a 150 m tower: 4, 8, 16, 32, 60, 91, 122, 150 m.

Table 3. Two-frequency microwave radiometer characteristics.

LO center frequencies	53.5 and 54.5 GHz
IF passband (2 dB)	10 to 110 MHz
sensitivity ($\tau=10$ s)	0.25 K
system noise figure*	11.4 dB
mixer noise figure	8.0 dB
antenna beamwidth (3 dB)	0.3°
estimated absolute accuracy	±3 K

* System noise figure is referred to the antenna input port.

TABLE 4. Root mean square difference [K] between measured brightness temperature and brightness temperature calculated from radiosonde data.

Date	Time	53.5 GHz	54.5 GHz
15 May	0515	3.41	2.21
	0815	2.53	1.69
	1937	2.63	1.96
16 May	0627	3.18	1.59
	0800	1.95	1.59
	1947	2.61	2.49
17 May	0516	3.29	4.07
	0800	2.90	1.63
	1935	2.44	1.97
18 May	0800	2.95	2.62
	1940	3.54	1.09
19 May	0510	2.43	2.62
	1000	3.27	1.16
rms difference for all measurements		2.92	2.19

TABLE 5. Average and root mean square difference [K] between measured and calculated brightness temperatures as a function of radiometer elevation angle.

Elevation angle (deg)	53.5 GHz Average	53.5 GHz rms	54.5 GHz Average	54.5 GHz rms
0	0	0	0	0
2.5	0.66	1.03	0.20	0.77
5	0.30	1.57	−0.40	1.01
7.5	0.04	2.00	−0.43	1.37
10	0.16	2.60	−0.63	1.64
12.5	0.32	2.67	−1.10	2.27
15	0.51	3.37	−0.94	2.44
20	1.78	3.42	−0.44	2.28
30	0.44	3.30	−0.46	2.77
40	0.69	2.69	0.08	1.97
50	−0.46	2.18	0.57	2.41
60	−1.99	2.74	0.14	2.02
70	−2.98	3.61	0.10	2.75
80	−3.95	4.50	0.07	2.36
90	−4.04	4.41	−1.54	3.18
All angles	−0.66	2.92	−0.34	2.19

Temperature sensors were copper-constantan thermocouples housed in aspirated radiation shields. Signals from the sensors were amplified at the tower and transmitted 680 m to a van where they were recorded on a digital tape recorder at a 10 Hz sampling rate. To reduce noise in the recorded temperatures, the sampled values were edited to remove each temperature that differed from the previous one by more than 1 K. The remaining samples were averaged over 1 min periods and then further smoothed by computing 10 min running averages; the latter values are plotted in Section 9.

Our radiosonde system was the standard rawin set AN/GMD1; temperature, humidity and wind data were recorded to a height of approximately 12 km above ground level. The radiosonde temperatures shown in Section 9 are significant level values.

A KIOWA helicopter contained sensors and recorders for air and soil temperatures; the latter quantity was measured with a downward looking infrared sensor. The air temperatures recorded on the helicopter are plotted in Section 9 with the profile comparisons.

9. Results

We now present the results of the measurements made at WSMR. We compare the brightness measurements with those calculated from theory, compare inferred and directly measured temperature profiles, and study the correlation between temperatures measured at various levels on the meteorological tower and microwave brightness measurements.

Thirteen temperature soundings using the brightness-vs-elevation-angle technique were made with simultaneous meteorological data. We first compare brightness temperatures calculated from radiosonde data (see Section 2) with measured brightness. Temperatures measured on the tower and helicopter are used as independent measures of the profile and its time variation rather than as input data for these brightness calculations. A summary of the measured and calculated theoretical brightness temperatures at 53.5 and 54.5 GHz is presented in Table 4 which lists the rms difference between measured and calculated quantities for the entire set of 15 elevation angles that comprise each run. Table 5 lists the average and rms difference between measurements and calculations as a function of antenna elevation angle; the averages are also shown in Fig. 9. A few individual sample comparisons are

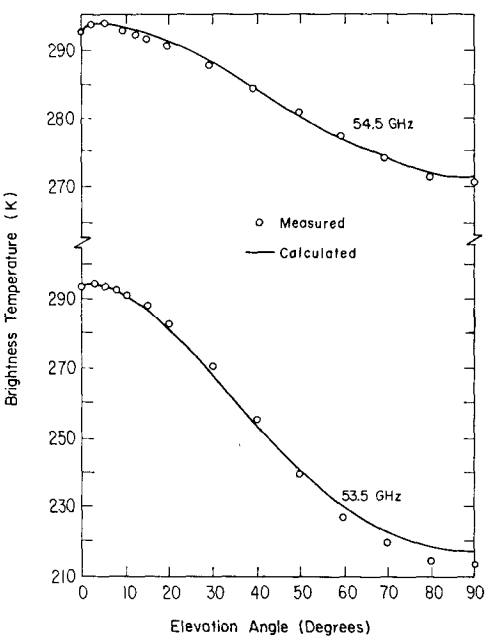

FIG. 9. Averages of measured and calculated microwave brightness for 13 profiles.

given in Figs. 10–12 which also include profile inversion results and meteorological tower temperatures that are discussed below.

Referring to Fig. 9 and Table 5, we see that agreement between measured and calculated brightness temperatures is good at 54.5 GHz and for elevation angles below 50° for 53.5 GHz. Some of the average disagreement between measurements and calculations may be caused by using an incorrect value for the stray antenna noise temperature as discussed in Section 7. Another possible cause, and one that would result in larger differences at the higher elevation angles, is incorrect absorption coefficients for H_2O and O_2.

Other possible sources of error, particularly during individual soundings, are departures from horizontal stratification and significant variation of the temperature profile during the time of measurement. The former did not seem to be important during this experiment since constant altitude helicopter flights (up to 1.5 km) indicated temperature variations of less than 1 K over a horizontal distance of $\sim$8 km. Similar observations during much more extreme surface temperature differences than we encountered were reported by Businger and Frisch (1972). They measured surface temperature differences of 20 K over an extended area. However, at 30 m, maximum differences in air temperature were less than 3 K over $\sim$10 km and at 100 m, the air temperature was homogeneous. We also grossly estimated the upper air horizontal temperature gradient from National Weather Service daily records of the 500 mb height contours. These records indicated maximum gradients of average temperature (to 500 mb) of less than 2×10^{-3}K km^{-1} during the week of the experiment.

As shown by the tower measurements, significant temporal variation of the temperature profile did occur at various times. Some of these cases will be discussed in detail later in this section.

Another source of error is the smoothing of low-altitude structure by the radiosonde. In several instances, the tower temperature measurements showed much more structure in the boundary layer than did the radiosonde. In all but one case, the first significant level that was reported by radiosondes was at least 100 m above the surface, while frequently much of the structure was actually below 30 m. Calculations of brightness using tower data spliced with radiosondes differed by as much as 1.5 K from those using only radiosonde data.

The cloud cover seen by the antenna main lobe during each temperature sounding was photographed and classified for subsequent qualitative estimates of effects upon the measurements. In general, cloud heights and estimated water content were such that contamination of the brightness data by cloud emission is believed to be extremely small.

We have enumerated some of the possible reasons for the observed differences in theory and experiment to indicate several limitations and uncertainties that remain in remote sensing of temperature profiles. For our immediate problem, the observed differences represent the measurement accuracy with which we must contend when estimating the temperature profile from a set of brightness data. On the basis of the average departure between measurements and theory, we have assigned a noise level of 1.0 K to the radiometer, i.e., the experimental error ε in (4) attributable to the radiometer is 1.0 K. Although the rms differences were larger than this, we felt that this larger variance was due to time variation of the profiles and did not represent radiometer error.

Temperature profiles were estimated from the brightness measurements by two methods: (a) the "exact" inversion algorithm employing Eqs. (2) through (6); and (b) the "approximate" method using Eqs. (3), (4), and (8) through (11). Input radiation data for the former method were the set of 30 measurements recorded at 53.5 and 54.5 GHz and the 15 angles listed in Table 5. The individual sets of 15 values measured at each frequency were the input data to the "approximate" inversion method; the limitation of 15 pieces of input data for the approximate method is the result of insufficient computer storage space. The statistical base from which regression coefficients, means and variances, etc. (required by both inversion algorithms) were computed, was the 5 year ensemble of WSMR radiosonde data mentioned in Section 3. The ensemble and the inversion results are independent of the 13 radiosonde profiles taken during 15–19 May 1972.

We present selected results of our profile retrievals beginning with Figs. 10–12. Part (a) of each figure shows the temperature profile (open circles) estimated by the exact procedure while the profiles measured by the radiosonde (solid line) and helicopter (crosses) are shown for comparison. The curves in part (b) present similar results for the approximate technique except that here the circles and crosses represent inferred temperatures from 53.5 and 54.5 GHz input data, respectively. The cloud type prevalent during each profile measurement is shown in parts (a) and (b). Part (c) shows measured (circles) and theoretical (lines) brightness temperatures corresponding to each inverted profile. Finally, tower temperature measurements are shown in part (d).

Fig. 10 illustrates the effect of a time-varying profile on the brightness spectrum. The first four measurements, 0° to 7.5°, were taken from 0515 to 0524 MDT 15 May 1972 while the inversion profile changed little with time. After calibration at 0527, the remaining measurements were made every 3 min from 0530 to 0600. As shown in (d), the low-altitude profile decreases to a minimum about 0545, then increases to a relative maximum again at 0600. As seen in (c), the brightness spectrum is in reasonable agreement with this trend, particularly at 54.5 GHz. The retrieved profiles, (a) and (b), reflect this feature by being close to the profile

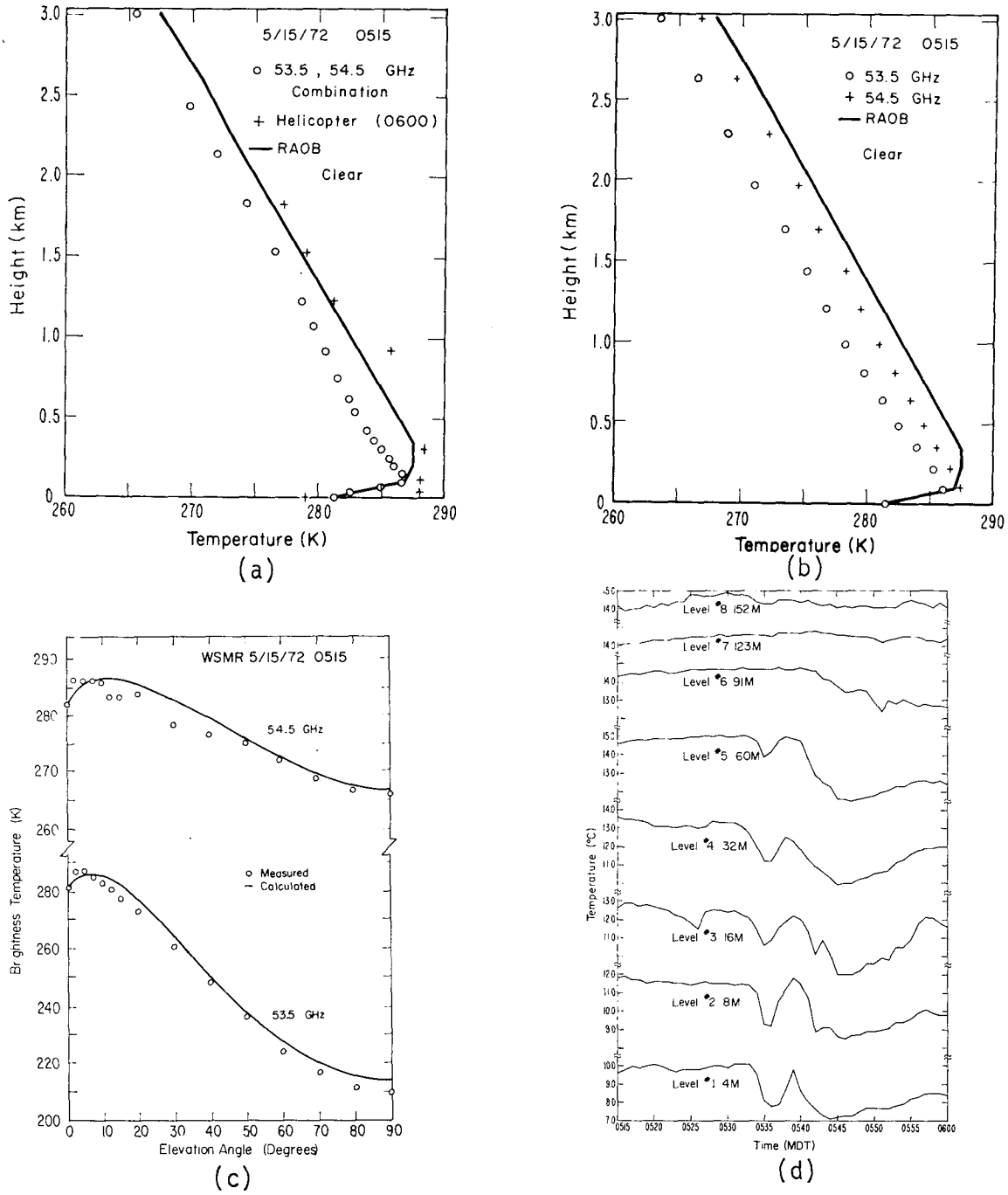

FIG. 10. Statistical inversion results for sounding begun 0515 MDT 15 May 1972. (See text for details.)

in the first several meters and then, at higher altitudes, become colder than the radiosonde profile.

Fig. 11 shows a profile retrieval from brightness measurements taken while the thermal profile (except for the first 8 m) changed little with time. The agreement between measurements and calculations is good, except for the angles above 60° at 53.5 GHz. The retrieved profiles well represent the radiosonde profile, particularly the retrieval obtained with 30 measurements.

The final case we present (Fig. 12) is an intense ground-based inversion. As is evident from the figure, the salient features of the thermal profile are well represented by the retrievals. Note that the retrieved profile is consistently warmer than the radiosonde pro-

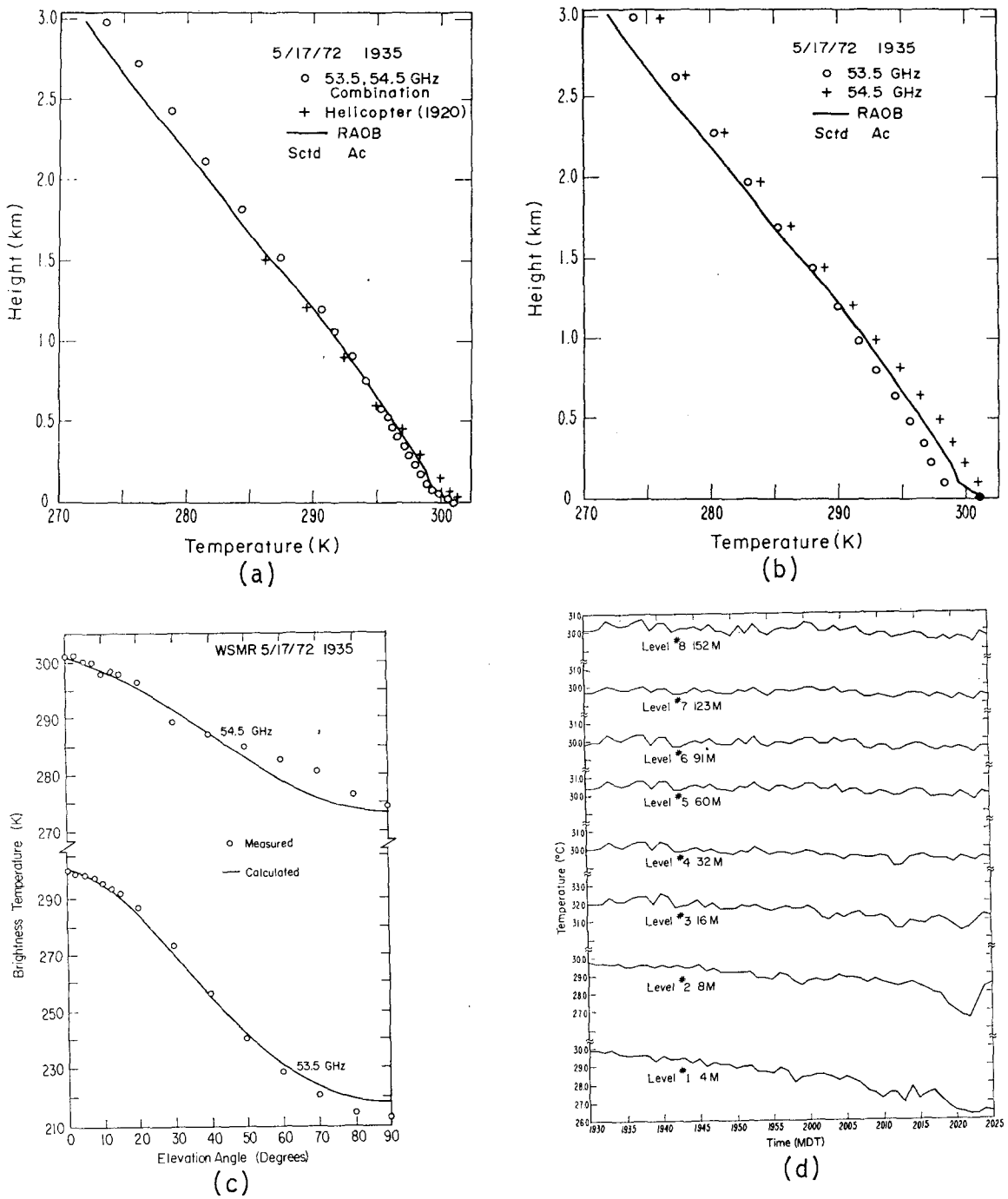

FIG. 11. As in Fig. 10 except for 1935 MDT 17 May 1972.

file above ~60 m. This could have been caused by the profile getting warmer with increasing time due to solar heating. Unfortunately, the tower measurements were unavailable during this period.

A total of 13 profiles were inverted for the one-week set of measurements. Table 6 summarizes the retrieval results for each profile as a function of inversion method and/or input data set; the tabulated values are the rms differences between estimated and radiosonde profiles. The reduction in variance by employing 30 brightness measurements instead of 15 is about 30%. In all cases of occurrence, ground-based inversions and lapse conditions were clearly indicated. The one elevated inversion that occurred was smoothed out in the re-

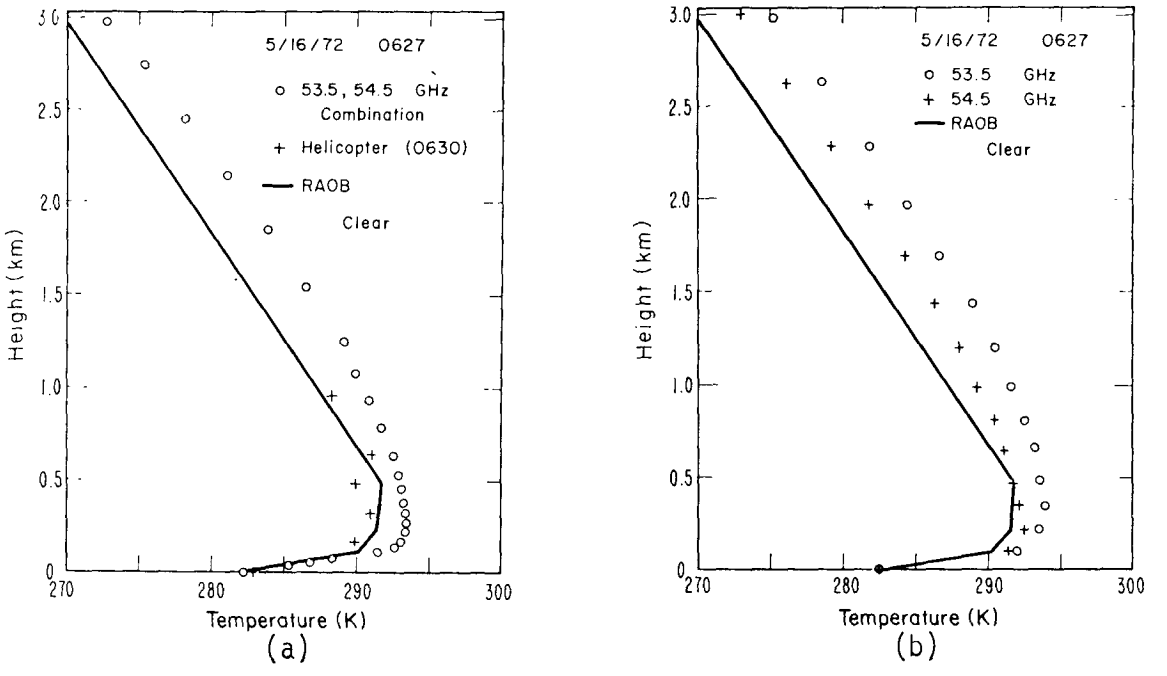

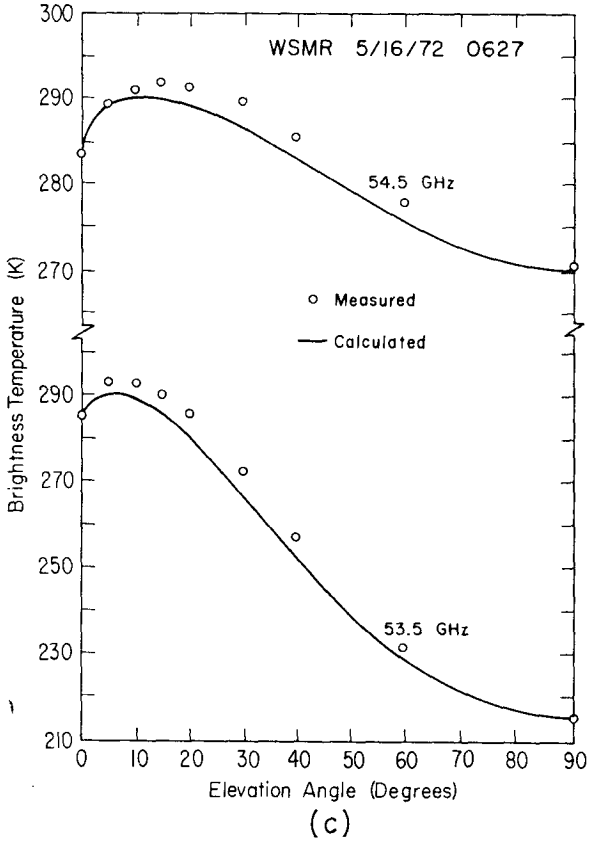

FIG. 12. As in Fig. 10 except for 0627 MDT 16 May 1972.

TABLE 6. Root mean square difference [K] between measured and inferred temperature profiles over 3 km height interval.

Date	Time	53.5 GHz (15 angles)	54.5 GHz (15 angles)	Both frequencies (15 angles)
15 May	0515	3.83	1.40	2.17
	0815	1.33	2.81	2.26
	1937	1.26	1.96	1.33
16 May	0627	4.17	2.13	2.31
	0800	0.98	2.40	1.24
	1947	0.53	3.03	2.47
17 May	0516	3.62	5.16	3.94
	0800	3.58	1.16	1.62
	1935	1.04	1.52	0.52
18 May	0800	0.90	1.64	1.47
	1940	0.67	1.54	0.58
19 May	0510	1.47	1.45	2.25
	1000	2.36	1.25	1.09
ΔT_{rms} for all profiles		2.36	2.36	1.99

trieval; however, these data were suspect because of strong radio interference, presumably due to tracking during a missile launch.

During the morning of 18 May, the microwave radiometer was operated at a fixed elevation angle for approximately 2½ h. The main purpose of this exercise was to investigate the degree of correlation between brightness at a fixed angle and the temperature measured at various levels on the meteorological tower; all microwave data were recorded at 5° elevation. Fig. 13 presents brightness temperatures at 53.5 and 54.5 GHz vs tower temperature at two levels. The sampling period was 5 min.

Note the relatively abrupt drop in microwave brightness temperature that coincides with the breakup of the inversion shortly after 0700. The observed behavior suggests the possibility that correctly interpreted direct brightness data at a fixed elevation angle may be a better indicator of atmospheric temperature at given heights than previously thought. Certainly, future experiments should evaluate this possibility by stressing brightness vs tower temperature measurements equally with angle scan measurements.

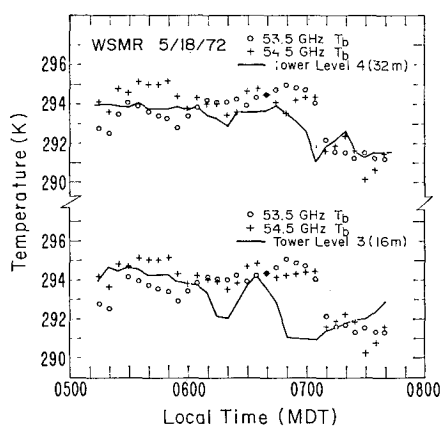

FIG. 13. Comparison of microwave brightness temperatures with tower temperatures at two levels.

10. Summary and conclusions

In this paper we have presented results of an experiment designed to compare direct and indirect soundings of vertical temperature profiles at White Sands Missile Range. Direct observations of temperature profiles were taken by radiosondes, by helicopters, and by sensors on a 150 m meteorological tower. Passive indirect soundings were obtained using a two-channel microwave radiometer operating at 53.5 and 54.5 GHz in the O_2 band. Statistical inversion of the microwave data resulted in an average rms temperature error of 2.0 K up to 3 km for 13 profiles.

The theoretical technique of Backus and Gilbert was applied to determine the vertical resolution or spread that can be achieved by our ground-based microwave radiometer operating in a variable elevation angle mode. The spread is an increasing function of altitude with values of ~75 m near the surface to ~1 km at a height of ~3 km. Theoretical estimates of accuracy in retrieving thermal profiles were less than 1.3 K up to about 3 km for radiometer noise levels of 1.0 K.

The microwave temperature retrievals exhibited generally good agreement with directly measured profiles. When there were significant departures between inferred and directly measured profiles, similar departures were present between calculations and measurements of brightness. Much of this discrepancy seems to be due to substantial changes in the low-altitude temperature profile during the period of measurements (~45 min). The available tower data tend to confirm this hypothesis. Comparison of tower data (when available) with plots of microwave brightness vs elevation angle revealed that temporal changes in the temperature profile were affecting the microwave data. Oscillations in temperature profiles gave rise to similar oscillations in the angular brightness curves. In several instances when the tower data were not available, similar features were present in the microwave plots. We may reasonably conclude that the present technique gives a poor representation of a temperature profile that is rapidly changing with time. On the other hand, the technique may give a better representation of the time-averaged temperature structure than a single radiosonde. The time required for a complete brightness scan could reasonably be reduced to 15 min with modifications of present equipment.

The ability of the microwave technique to indicate the presence or absence of ground-based temperature inversions was successfully demonstrated. In most cases, the inversion heights are accurately recovered; some differences in radiosonde and inferred measurements of

the inversion intensity may be the result of rapidly changing profiles as discussed above.

The correlation between fixed angle brightness and tower temperatures at a fixed height was quite good. Future experiments should gather a much larger data base under a wide variety of profile conditions to determine to what degree and on what time scale these fluctuations can be correlated.

The success of the radiometer to retrieve, with a resolution that degrades with height, smoothed features of the thermal profile suggests that the technique could supplement satellite soundings in the first 300 mb above the surface. An automated system, with a microwave window channel, could be used in remote regions to provide profile information routinely, except during precipitation. Research is currently underway to determine the feasibility of radiometric sensing of temperature profiles from ocean-based data buoys.

Acknowledgments. The authors acknowledge Dr. Sterling E. Taylor for the operation of the helicopter in gathering temperature data. We thank Marvin A. Hamiter who was responsible for installation and operation of the meteorological tower. R. S. Lawrence offered helpful suggestions on the manuscript.

REFERENCES

Backus, G., and F. Gilbert, 1970: Uniqueness in the inversion of inaccurate gross earth data. *Phil. Trans. Roy. Soc. London*, **266**, 123–192.

Businger, J. A., and A. S. Frisch, 1972: Cold plumes. *J. Geophys. Res.*, **77**, 3270–3271.

Carter, C. J., R. L. Mitchell and E. E. Reber, 1968: Oxygen absorption measurements in the lower atmosphere. *J. Geophys. Res.*, **73**, 3121–3127.

Colin, L., Ed., 1972: *Proc. Workshop on Mathematics of Profile Inversion*, Ames Res. Center, Moffett Field, Calif., NASA Tech. Memo. TM X-62, 150 pp.

Conrath, B. J., 1972: Vertical resolution of temperature profiles obtained from remote radiation measurements. *J. Atmos. Sci.*, **29**, 1262–1271.

Deutsch, R., 1965: *Estimation Theory*. Englewood, Cliffs, N. J., Prentice-Hall, Inc., 269 pp.

Dicke, R. H., 1946: The measurement of thermal radiation at microwave frequencies. *Rev. Sci. Instr.*, **17**, 268–275.

Miner, G. F., D. D. Thornton and W. J. Welch, 1972: The inference of atmospheric temperature profiles from ground-based measurements of microwave emission from atmospheric oxygen. *J. Geophys. Res.*, **77**, 975–991.

Morrison, D. F., 1967: *Multivariate Statistical Methods*. McGraw-Hill, 338 pp.

Mount, W. D., B. R. Fow, C. V. Wick and C. M. Maloy, 1969: Three radiometric data analysis techniques for measuring air temperature profiles. Sperry Rand Research Center, Sudbury, Mass., Report under Contract CPA 22-69-116, prepared for Air Pollution Control Office, EPA, Durham, N. C.

Snider, J. B., 1972: Ground-based sensing of temperature profiles from angular and multi-spectral microwave emission measurements. *J. Appl. Meteor.*, **11**, 958–967.

——, 1974: A sensitive two-frequency radiometer for remote sensing of temperature profiles. *Rev. Sci. Instr.*, **45**, 981–984.

Staelin, D. H., A. H. Barrett, J. W. Waters, F. T. Barath, E. J. Johnson, P. W. Rosenkranz, N. E. Gaut and W. B. Lenoir, 1973: Microwave spectrometer on the Nimbus 5 satellite: Meteorological and geophysical data. *Science*, **181**, 1339–1341.

Waters, J. W., 1971: Ground-based passive microwave sensing of temperatures in the stratosphere and lower mesosphere. *Proc. 7th Intern. Symp. Remote Sensing of Environment*, Ann Arbor, Mich., 1765–1776.

Westwater, E. R., 1967: An analysis of the correction of range errors due to atmospheric refraction by microwave radiometric techniques. ESSA Tech. Rept. IER 37-ITSA 37.

——, 1972a: Ground-based determination of low-altitude temperature profiles by microwaves. *Mon. Wea. Rev.*, **100**, 15–28.

——, 1972b: Microwave emission from clouds. NOAA Tech. Rept. ERL-219 WPL-18, 55 pp.

——, and A. Cohen, 1973: Application of Backus-Gilbert inversion technique to determination of aerosol size distributions from optical scattering measurements. *Appl. Opt.*, **12**, 1340–1348.

——, J. B. Snider, A. V. Carlson and J. R. Yoder, 1973: Experimental determination of temperature profiles by ground-based radiometry. NOAA Tech. Rept. ERL-289 WPL 27.

——, and O. N. Strand, 1968: Statistical information content of radiation measurements used in indirect sensing. *J. Atmos. Sci.*, **25**, 750–758.

——, and ——, 1972: Inversion techniques. *Remote Sensing of the Troposphere*. V. E. Derr, Ed., U. S. Govt. Printing Office, Washington, D. C., Chap. 16.